Supplemental Material

Genome-wide profiling reveals functional interplay of DNA sequence composition, transcriptional activity, and nucleosome positioning in driving DNA supercoiling and helix destabilization in *C. elegans* embryos

Kristina Krassovsky,[1] Rajarshi P. Ghosh,[1,2] and Barbara J. Meyer[1,2]

[1]Department of Molecular and Cell Biology
University of California, Berkeley
Berkeley, California 94720-3204, USA

[2]Howard Hughes Medical Institute

Corresponding Author:
Barbara J. Meyer
Email: bjmeyer@berkeley.edu
Tel.: +1 510-643-5585

Running Title:
Genome-wide mapping of DNA supercoiling and SS DNA

Key words:
DNA Supercoiling, Single-Stranded DNA, Nucleosome Positioning,
X-Chromosome Dosage Compensation,
Biotinylated Psoralen Photo-Crosslinking,
Potassium Permanganate Reactivity, *Caenorhabditis elegans*

Table of Contents

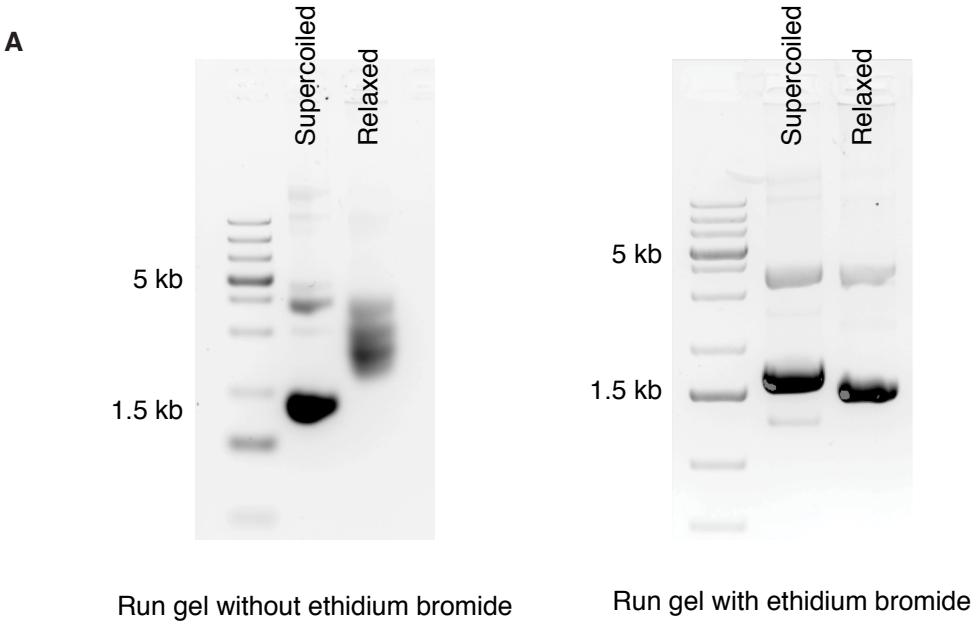
A
Supercoiled
Relaxed
5 kb
1.5 kb
Run gel without ethidium bromide
Supercoiled
Relaxed
5 kb
1.5 kb
Run gel with ethidium bromide

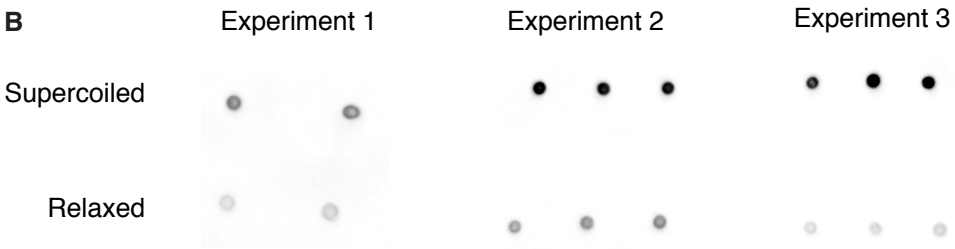
B
Experiment 1
Experiment 2
Experiment 3
Supercoiled
Relaxed

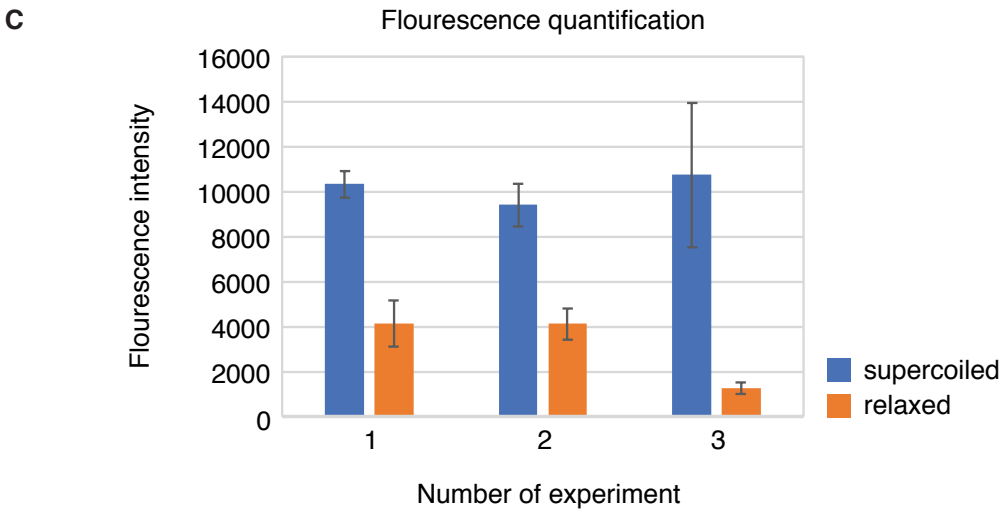
C
Flourescence quantification
Flourescence intensity
16000
14000
12000
10000
8000
6000
4000
2000
0
1
2
3
Number of experiment
supercoiled
relaxed

Supplemental Figure S1. Biotinylated psoralen (BP) incorporates preferentially into negatively supercoiled DNA.

(*A*) Images of supercoiled and relaxed plasmid DNA electrophoresed through agarose gels in the absence and presence of ethidium bromide to verify the supercoiling status of DNA.

(*B*) Representative dot blot images of supercoiled and relaxed plasmids incubated with BP and probed with streptavidin-conjugated horseradish peroxidase.

(*C*) Quantification of fluorescence in dot blots exemplified in (*B*) verifies preferential BP incorporation into supercoiled DNA versus relaxed DNA.

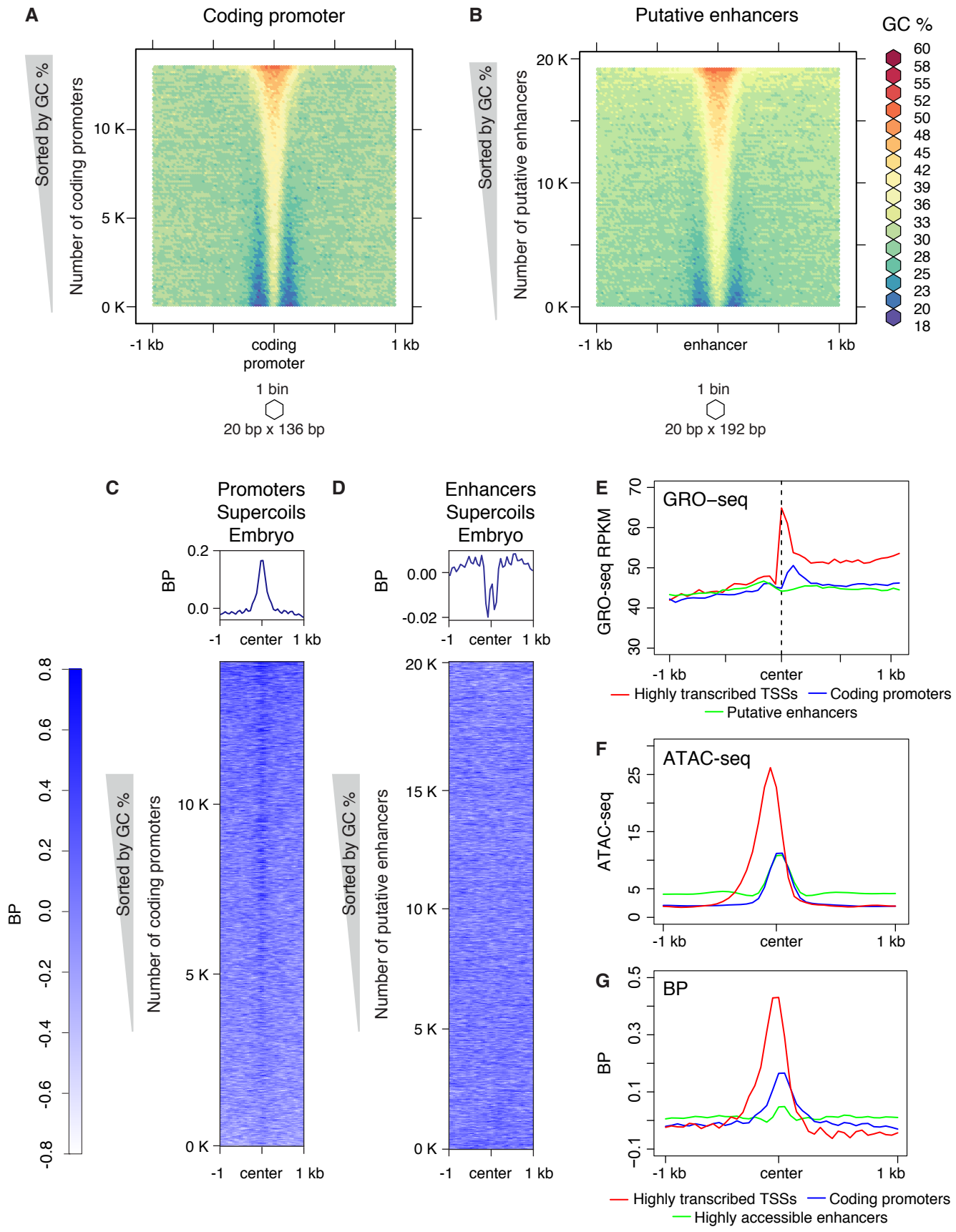
A
Coding promoter
Sorted by GC %
Number of coding promoters
10 K
5 K
0 K
-1 kb
coding promoter
1 kb
1 bin
20 bp x 136 bp
B
Putative enhancers
GC %
60
58
55
52
50
48
45
42
39
36
33
30
28
25
23
20
18
Sorted by GC %
Number of putative enhancers
20 K
10 K
0 K
-1 kb
enhancer
1 kb
1 bin
20 bp x 192 bp
C
Promoters
Supercoils
Embryo
BP
0.2
0.0
-1
center
1 kb
BP
0.8
0.6
0.4
0.2
0.0
-0.2
-0.4
-0.6
-0.8
Sorted by GC %
Number of coding promoters
10 K
5 K
0 K
-1
center
1 kb
D
Enhancers
Supercoils
Embryo
BP
0.00
-0.02
-1
center
1 kb
Sorted by GC %
Number of putative enhancers
20 K
15 K
10 K
5 K
0 K
-1
center
1 kb
E
GRO−seq
GRO-seq RPKM
70
60
50
40
30
-1 kb
center
1 kb
Highly transcribed TSSs
Coding promoters
Putative enhancers
F
ATAC-seq
ATAC-seq
25
15
5
0
-1 kb
center
1 kb
G
BP
BP
0.5
0.3
0.1
−0.1
-1 kb
center
1 kb
Highly transcribed TSSs
Coding promoters
Highly accessible enhancers

Supplemental Figure S2. Open chromatin is not the primary determinant of psoralen binding.

(*A*) (*B*) Heatmaps of GC content in the 2 kb region around (*A*) 13,596 low-to-moderately transcribed coding promoters and (*B*) 19,231 putative enhancers reveal GC-rich regions with sharp GC/AT boundaries.

(*C*) Heatmap of supercoils (wild-type embryos, replicate 1) in the coding promoters shown in (*A*) recapitulate the findings of Figure 2 showing that the boundaries of supercoiling at TSSs are marked by a sharp GC to AT transition.

(*D*) Heatmap of supercoils in the 2 kb region surrounding putative enhancers shown in (*B*) reveals little or no supercoiling, correlated with the lack of transcription at these putative enhancer sites. The center of each enhancer was defined by the center of the ATAC-seq peak. The heatmaps for GC content were made as in Figure 2A, but with the bin for promoters being 20 bp × 136 bp, and the bin for enhancers being 20 bp × 192 bp.

(*E*) GRO-seq counts at the 13,596 coding promoters (blue) and 19,231 putative enhancers (green) are compared with GRO-seq counts at the TSSs of 4221 highly transcribed genes (red).

(*F*) Average profiles of ATAC-seq signal in embryos are plotted for the 2 kb region surrounding coding promoters (13,596), highly accessible putative enhancers (9677), and TSSs of highly transcribed genes (4221) at 50 bp resolution.

(*G*) Average profiles of BP-seq in embryos is plotted for a 2 kb region around coding promoters (13,596), highly accessible putative enhancers (9677), and TSSs of highly transcribed genes (4221) at 50 bp resolution.

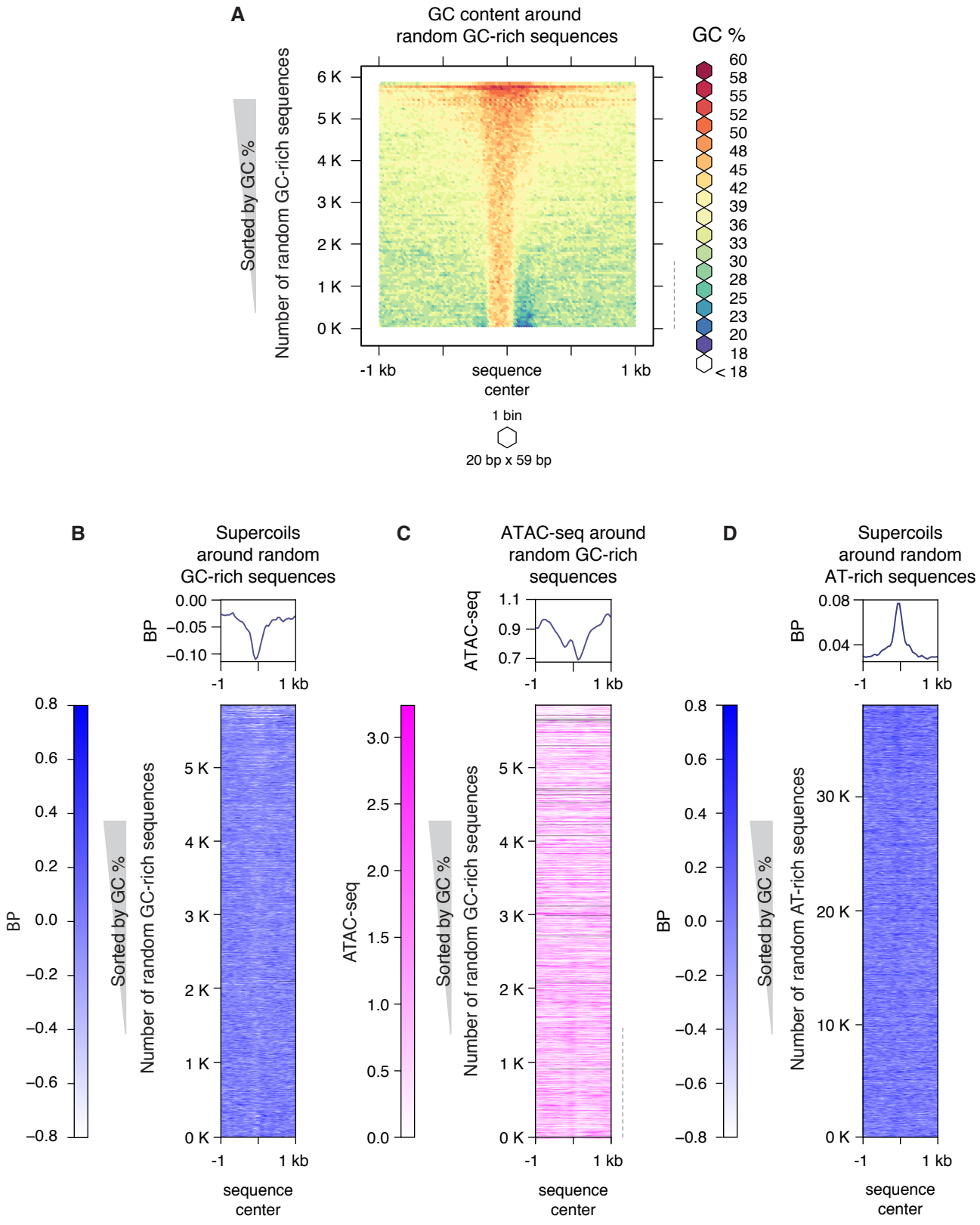
A
GC content around
random GC-rich sequences
GC %
60
58
55
52
50
48
45
42
39
36
33
30
28
25
23
20
18
< 18
Sorted by GC %
Number of random GC-rich sequences
6 K
5 K
4 K
3 K
2 K
1 K
0 K
-1 kb
sequence
center
1 kb
1 bin
20 bp x 59 bp
B
Supercoils
around random
GC-rich sequences
BP
0.00
−0.05
−0.10
-1
1 kb
0.8
0.6
0.4
0.2
0.0
−0.2
−0.4
−0.6
−0.8
Sorted by GC %
Number of random GC-rich sequences
5 K
4 K
3 K
2 K
1 K
0 K
sequence
center
C
ATAC-seq around
random GC-rich
sequences
ATAC-seq
1.1
0.9
0.7
3.0
2.5
2.0
1.5
1.0
0.5
0.0
D
Supercoils
around random
AT-rich sequences
0.08
0.04
Number of random AT-rich sequences
30 K
20 K
10 K

Supplemental Figure S3. Random GC-rich sequences lack negative supercoiling and have weaker GC/AT boundaries than GC-rich sequences of coding promoters, putative enhancers and highly active TSSs.

(*A*) Heatmap of GC content around 5,862 random GC-rich (GC % >0.45) sequences. Sequences were sorted by their GC content, aligned on top of each other, and binned at 20 bp × 59 bp. To select DNA for the heatmap, 400 bp DNA sequences with an average GC content greater than 45% were identified, 1 kb was added to each side, and sequences were aligned at the center of the original 400 bp region. Each bin was colored according to its GC percentage. These random GC-rich regions have weaker GC/AT boundaries than promoters. The dashed line highlights the sequences with strong GC/AT boundaries.

(*B*) Heatmap of supercoils for wild-type embryos (replicate 1) at random GC-rich sequences does not reveal negative supercoiling.

(*C*) Heatmap of ATAC-seq profile around random GC-rich sequences. The dashed line highlights the ATAC-seq signal at sequences with strong GC/AT boundaries.

(D) Heatmap of supercoils for wild-type embryos (replicate 1) around random AT-rich sequences shows greatly attenuated BP-seq signal.

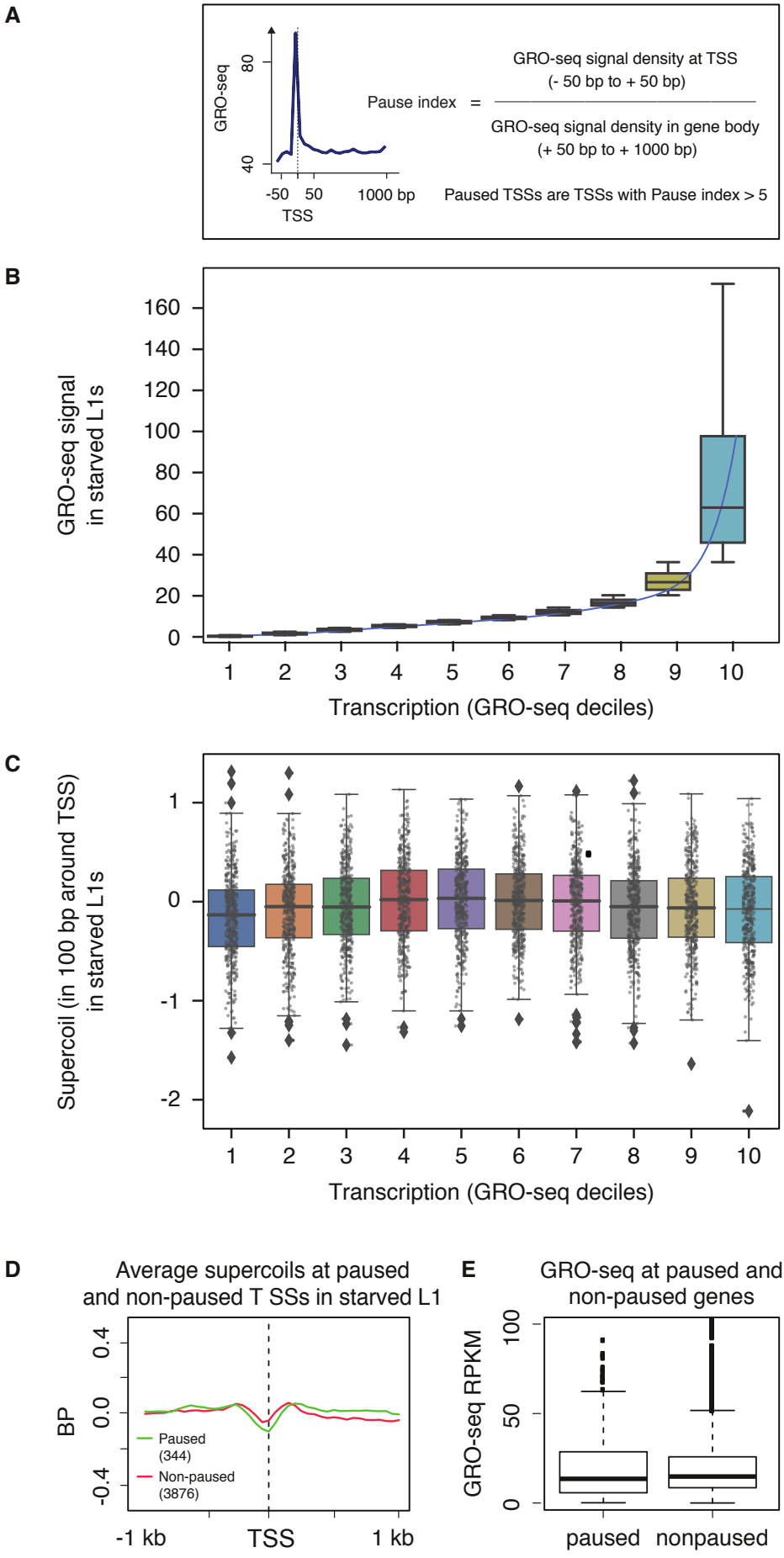
A
GRO-seq
80
40
-50
50
1000 bp
TSS
Pause index =
GRO-seq signal density at TSS
(- 50 bp to + 50 bp)
GRO-seq signal density in gene body
(+ 50 bp to + 1000 bp)
Paused TSSs are TSSs with Pause index > 5
B
GRO-seq signal
in starved L1s
Transcription (GRO-seq deciles)
C
Supercoil (in 100 bp around TSS)
in starved L1s
Transcription (GRO-seq deciles)
D
Average supercoils at paused
and non-paused T SSs in starved L1
BP
Paused
(344)
Non-paused
(3876)
-1 kb
TSS
1 kb
E
GRO-seq at paused and
non-paused genes
GRO-seq RPKM
paused
nonpaused

Supplemental Figure S4. TSSs in starved L1 larvae have attenuated BP-seq signal and exhibit similar supercoiling profiles with and without RNA Pol II pausing.

(*A*) Formula for determining the pause index of a TSS. More paused genes occur in starved L1s than other developmental stages (Baugh and Sternberg 2006; Kruesi et al. 2013).

(*B*) Box and whisker plots of GRO-seq values for 4221 genes in starved L1 larvae after partitioning into deciles based on their average GRO-seq signal in the gene body. The lowest decile (decile 1) includes genes with the lowest 10% of GRO-seq values. A trend line through the medians of box plots for each decile shows a graded increase in GRO-seq values up to decile 6, followed by a much sharper ascent from deciles 7 to 10, similar to the trend seen in embryos (Figure 2D).

(*C*) Box and whisker plots of BP-seq signal in 100 bp intervals around TSSs correspond to the GRO-seq deciles shown in (*B*). BP-seq signal is generally not correlated with transcription level in starved L1 larvae.

(*D*) BP-seq profile at 50 bp resolution in the 2 kb region around TSSs with paused (344 TSSs) and non-paused (3876 TSSs) transcription.

(*E*) GRO-seq signal in bodies of genes having paused and non-paused transcription in starved L1s.

A

$$\text{TMP} = \frac{\text{TMP nuclear DNA}}{\text{TMP genomic DNA}}$$

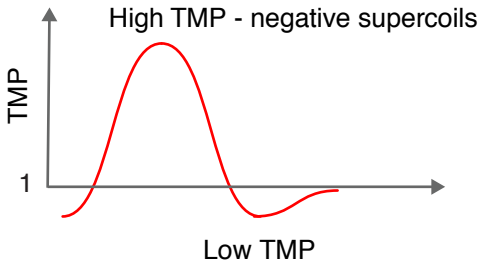

B Average supercoiling at active human TSS

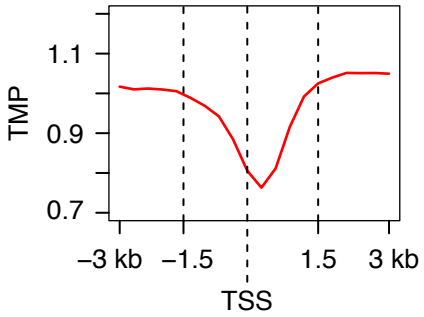

C GC content around active human TSSs

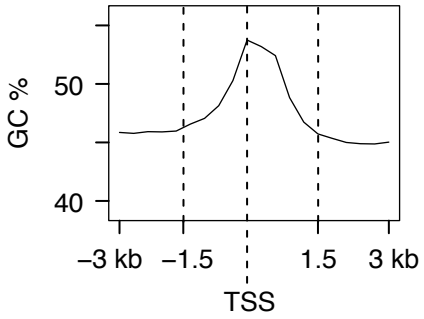

D Average supercoiling at fly TSSs

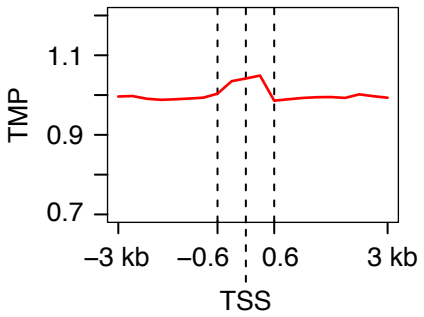

E GC content around fly TSSs

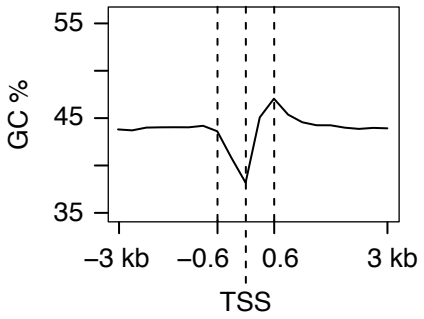

Supplemental Figure S5. Comparison of supercoiling profiles and GC content at TSSs of human and fly cell lines reveal common regulatory themes.

(*A*) Supercoiling is quantified by the ratio of nuclear DNA with incorporation of 4,5',8-trimethylpsoralen (TMP) versus naked genomic DNA with TMP incorporation. High TMP incorporation indicates negative supercoils. To create supercoiling plots around TSSs, the ratio of TMP reads in nuclear DNA of cells versus naked genomic DNA was normalized to the average signal around each TSS in a 6 kb region.

(*B*) The average supercoiling profile at TSSs of 13,226 highly expressed genes in human mammary epithelial MCF10A cells shows a peak of positive supercoils, with an average spread of 3 kb.

(*C*) Average GC content around TSSs of highly expressed human genes in (*B*). The extent of high GC content at TSSs corresponds to the propagation of positive supercoils at these TSSs.

(*D*) Analysis of supercoiling at 13,883 TSSs in *Drosophila melanogaster* S2 cells reveals a peak of negative supercoils with an average spread of 1.2 kb.

(*E*) Average GC content around TSSs of S2 cells shown in (*D*) shows that AT-rich regions at TSSs marked by a sharp transition to GC-rich regions delineate the boundary of supercoiling.

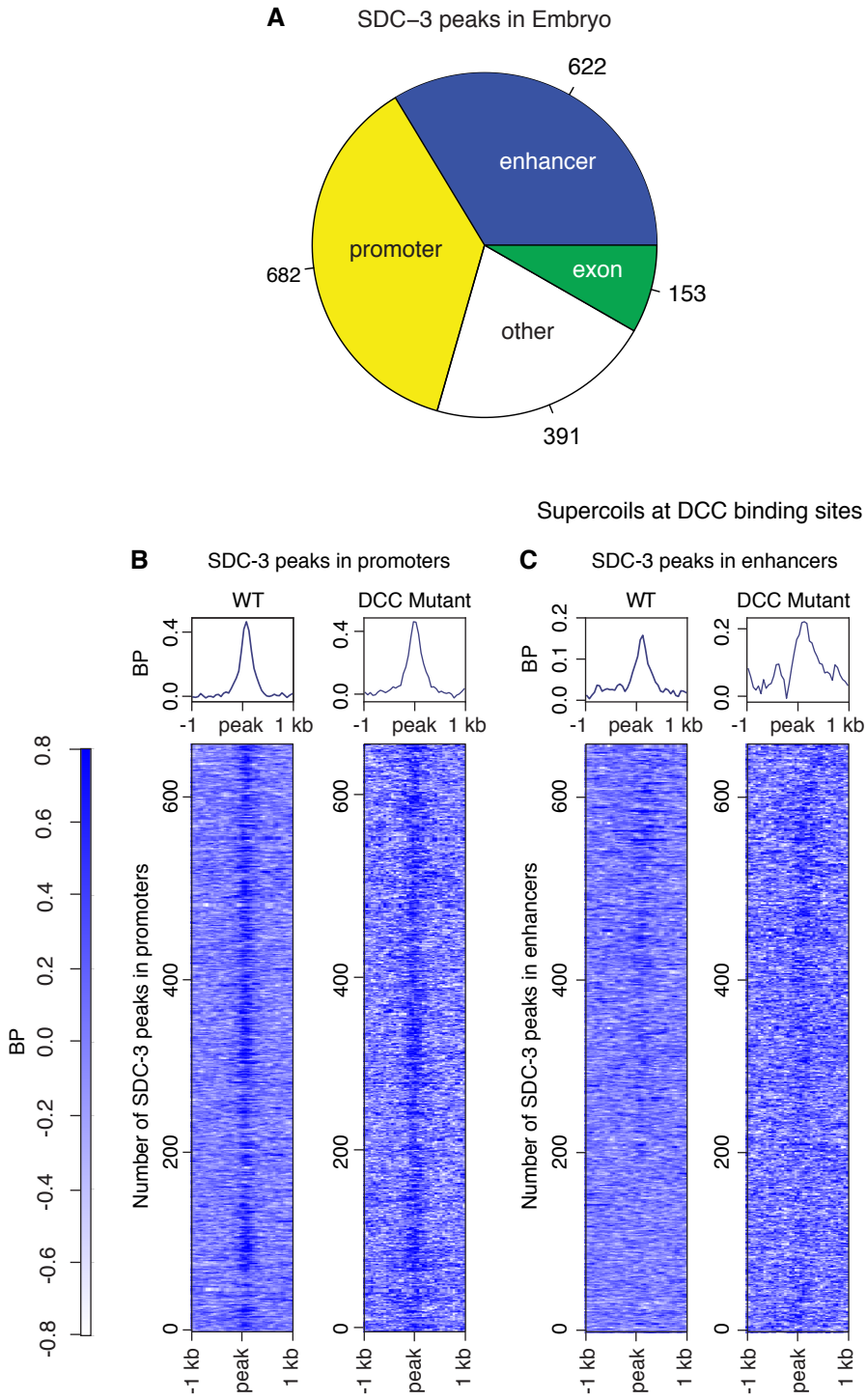
A
SDC–3 peaks in Embryo
622
enhancer
promoter
682
exon
153
other
391
Supercoils at DCC binding sites
B
SDC-3 peaks in promoters
C
SDC-3 peaks in enhancers
WT
DCC Mutant
BP
-1 peak 1 kb
Number of SDC-3 peaks in promoters
Number of SDC-3 peaks in enhancers
-1 kb
peak
1 kb

Supplemental Figure S6. Supercoiling profiles at secondary, non-autonomous DCC binding sites, located primarily in promoters and enhancers, correlate with transcriptional status of the sites and do not change upon disruption of DCC binding.

(*A*) The pie chart classifies 1848 different secondary binding sites of DCC subunit SDC-3 by location in enhancers, promoters, other ATAC-seq peaks, and exons.

(*B*) (*C*) Heatmaps of supercoils are plotted at 50 bp resolution in the 2 kb region around secondary DCC binding sites of wild-type (replicate 1) and DCC-mutant embryos (*sdc-2* mutant, replicate 1). DCC binding sites are grouped by their presence in promoters (*B*) or enhancers (*C*).

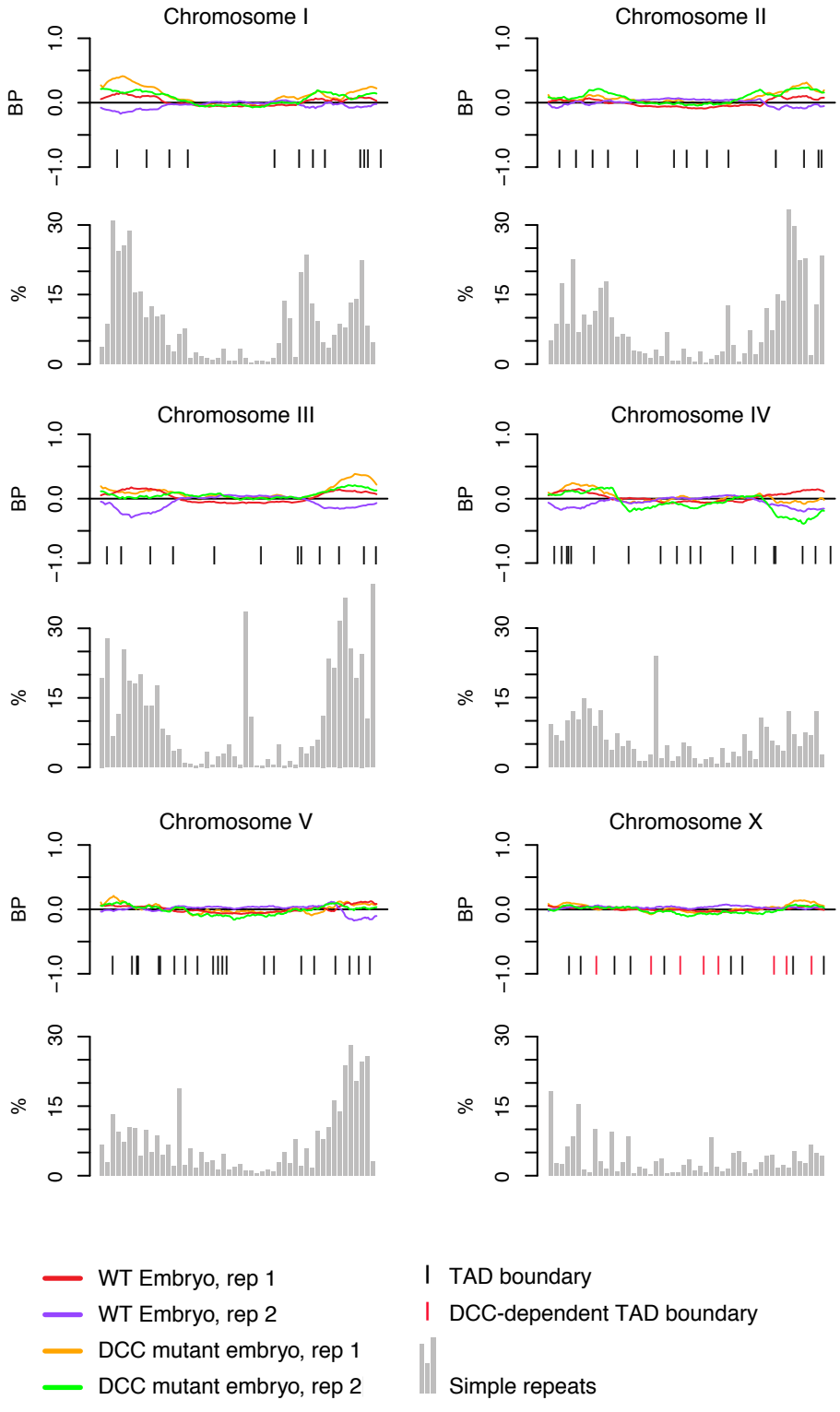
Chromosome I
Chromosome II
Chromosome III
Chromosome IV
Chromosome V
Chromosome X
BP
%
1.0
0.0
−1.0
30
15
0
WT Embryo, rep 1
WT Embryo, rep 2
DCC mutant embryo, rep 1
DCC mutant embryo, rep 2
TAD boundary
DCC-dependent TAD boundary
Simple repeats

Supplemental Figure S7. The dosage compensation complex does not create supercoiling domains on X-Chromosomes.

For each X-Chromosome and each autosome, BP-seq signal for wild-type and DCC mutant embryos was averaged over 1 kb sliding windows and plotted. TAD boundaries and percentage of simple repeats are shown under each chromosome. Chromosome regions enriched in simple repeats exhibit higher variation in BP signal between experiments, likely due to variable amplification during library preparation. *C. elegans* lacks large-scale supercoiling domains on any chromosome, and TAD boundaries are not enriched for supercoils.

SS-seq - a method to map single-stranded DNA.

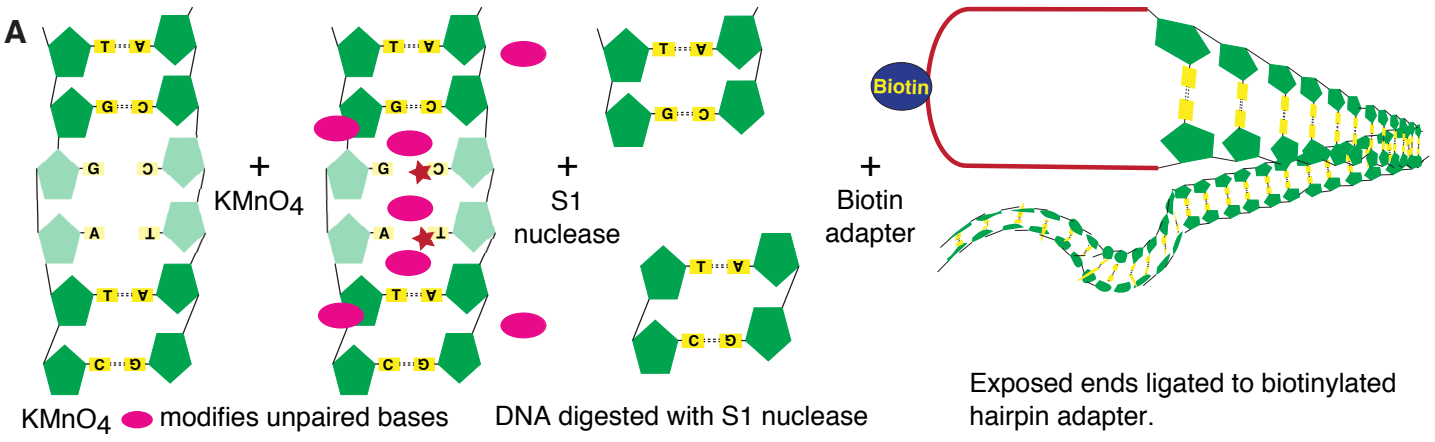

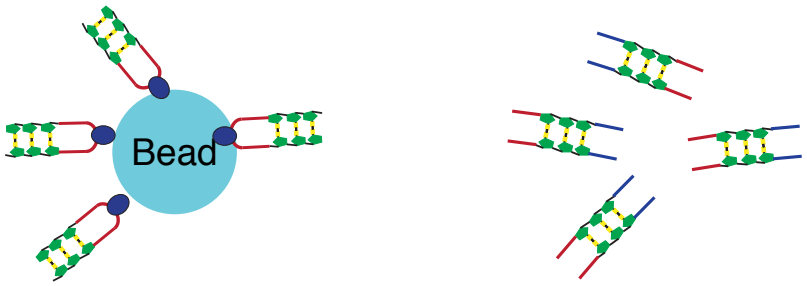

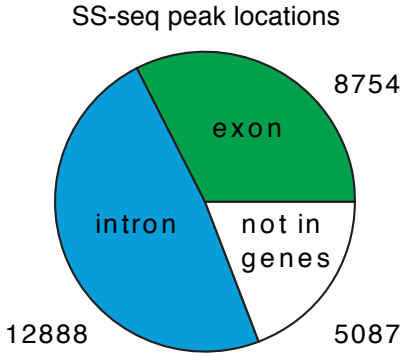

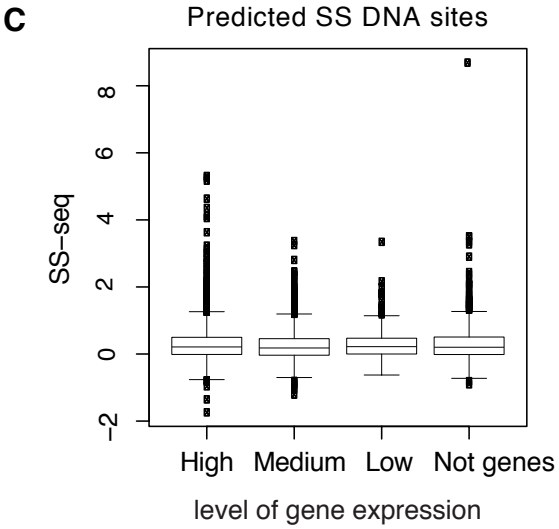

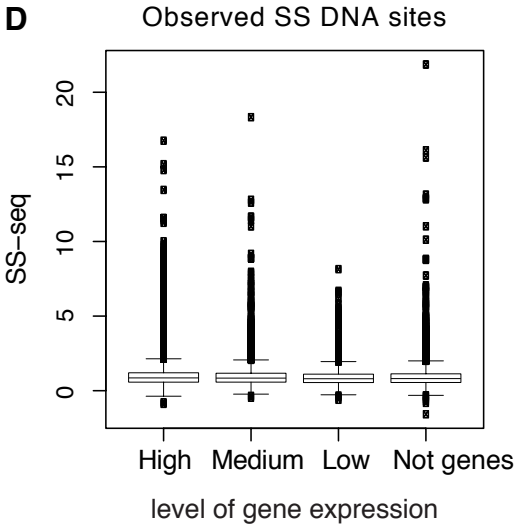

Distribution of the nucleosome distances around predicted and observed SS DNA sites

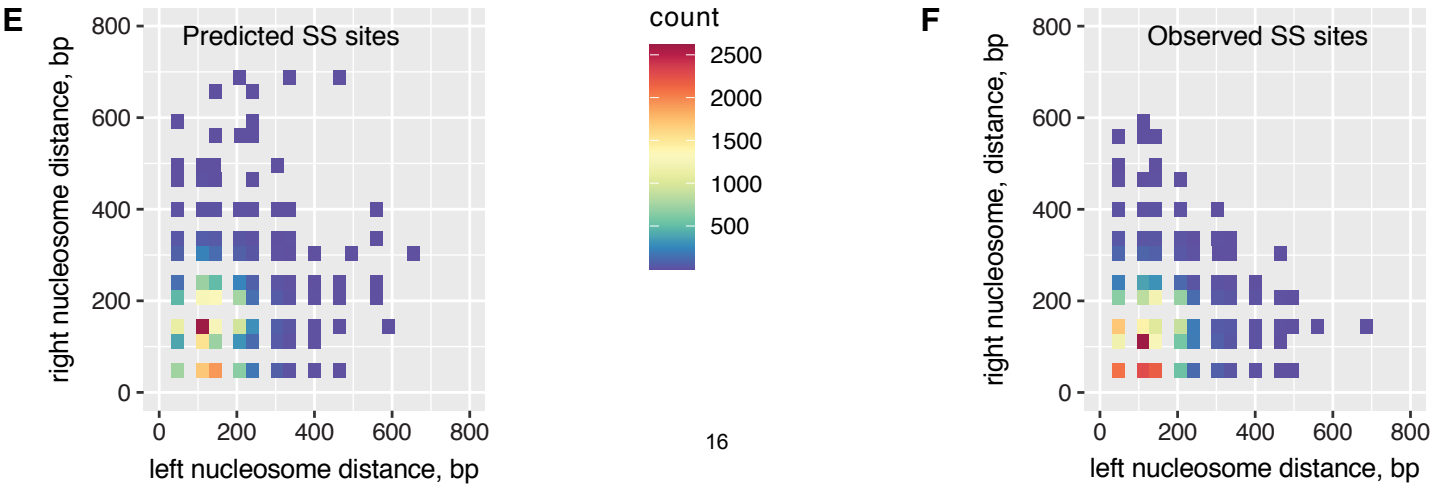

Supplemental Figure S8. SS-seq signal is decoupled from transcription but is strongly correlated with nucleosome positioning.

(*A*) Method to map single-stranded DNA and other non-B forms of DNA.

When $KMnO_4$ enters purified nuclei, it modifies unpaired pyrimidine bases and thereby prevents their reannealing, creating stable SS DNA. Purified DNA is digested with the single-strand-specific S1 nuclease, and exposed DNA ends are ligated to biotinylated hairpin adapters. Following DNA sonication to 300 bp, biotinylated DNA ends are enriched on streptavidin beads, and a second set of adapters is ligated. After digestion of adapter hairpins, the library is amplified and sequenced. The same procedure is applied to naked genomic DNA as a control. The distribution of the difference of counts from $KMnO_4$-treated nuclear DNA and genomic control DNA is calculated genome wide.

(*B*) Pie chart shows the distribution and number of SS-seq peaks in exons, introns, and extragenic regions.

(*C*) (*D*) Predicted (*C*) and Observed (*D*) SS DNA sites were classified by their presence in low, medium, or highly expressed genes or in extragenic sites. Cumulative SS-seq signal in a 100 bp window around the center of each SS-seq peak was calculated. Box plots show distribution of cumulative SS-seq signal for peaks coincident with each gene expression category or extragenic sites.

(*E*) (*F*) Symmetric nucleosomes occur at a higher frequency in observed SS-seq peaks than in predicted SS DNA sites. Shown are 2D histograms of distances between nucleosomes nearest to the right or left of SS DNA in predicted (*E*) and observed (*F*) sites.

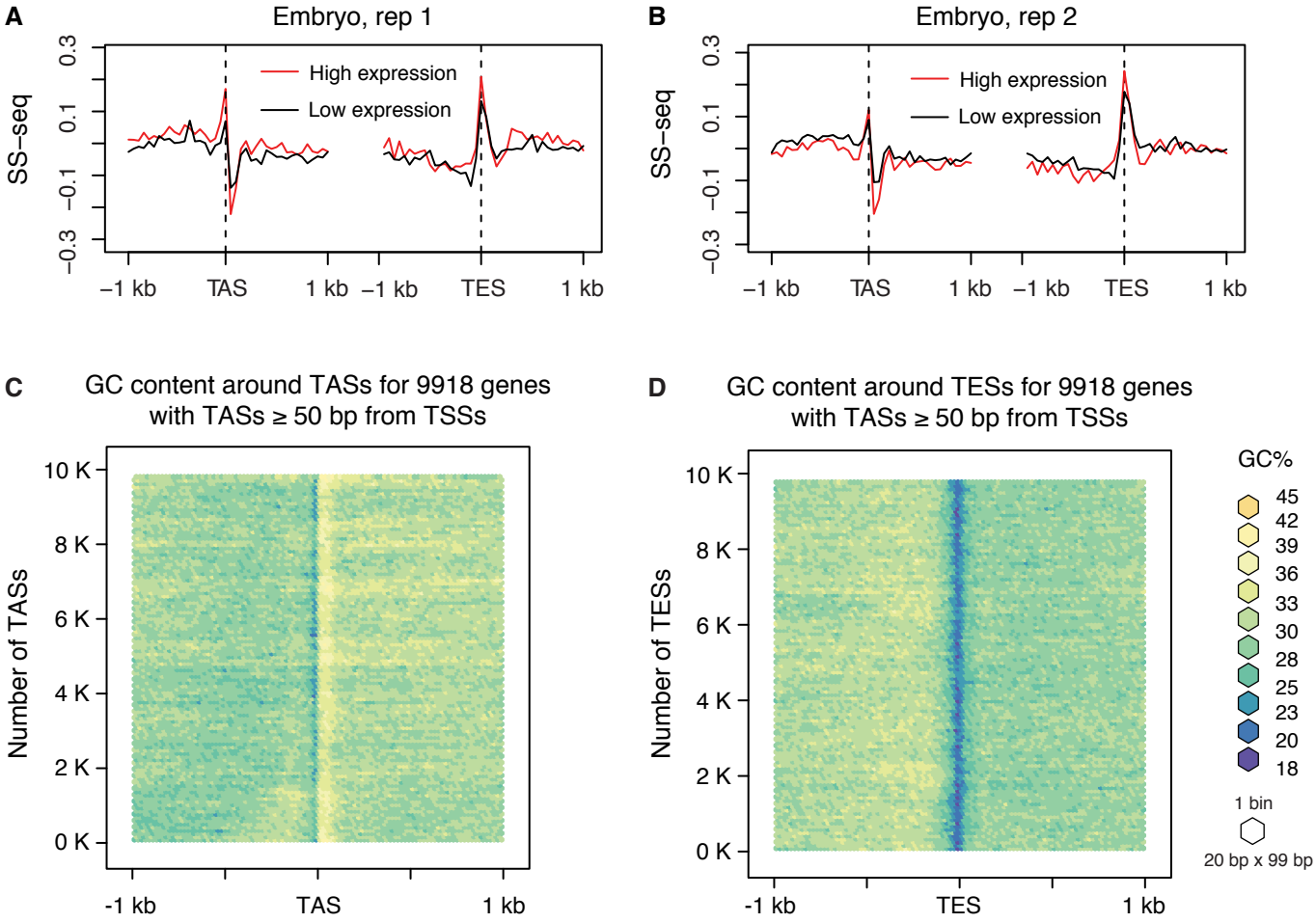
A
Embryo, rep 1
SS−seq
0.3
0.1
−0.1
−0.3
High expression
Low expression
−1 kb
TAS
1 kb
−1 kb
TES
1 kb
B
Embryo, rep 2
SS−seq
0.3
0.1
−0.1
−0.3
High expression
Low expression
−1 kb
TAS
1 kb
−1 kb
TES
1 kb
C
GC content around TASs for 9918 genes
with TASs ≥ 50 bp from TSSs
Number of TASs
10 K
8 K
6 K
4 K
2 K
0 K
-1 kb
TAS
1 kb
D
GC content around TESs for 9918 genes
with TASs ≥ 50 bp from TSSs
Number of TESs
10 K
8 K
6 K
4 K
2 K
0 K
-1 kb
TES
1 kb
GC%
45
42
39
36
33
30
28
25
23
20
18
1 bin
20 bp x 99 bp

Supplemental Figure S9. SS-seq signal scales with AT content at TESs and TASs, but not with levels of transcription.

(*A*) (*B*) Average SS-seq profiles are plotted at 50 bp resolution in the 2 kb regions surrounding TASs and TESs for high (3307 genes) and low (3306 genes) expression genes.

(C) (D) Heatmap of GC content in the 2 kb region around TASs (*C*) and TESs (*D*) of 9,918 genes reveals a minor increase in AT content at TASs and a robust increase at TESs.

Pearson correlation between pairwise combinations of BP-seq datasets in 500 bp windows around TSSs of the 4223 genes analyzed in Figure 2

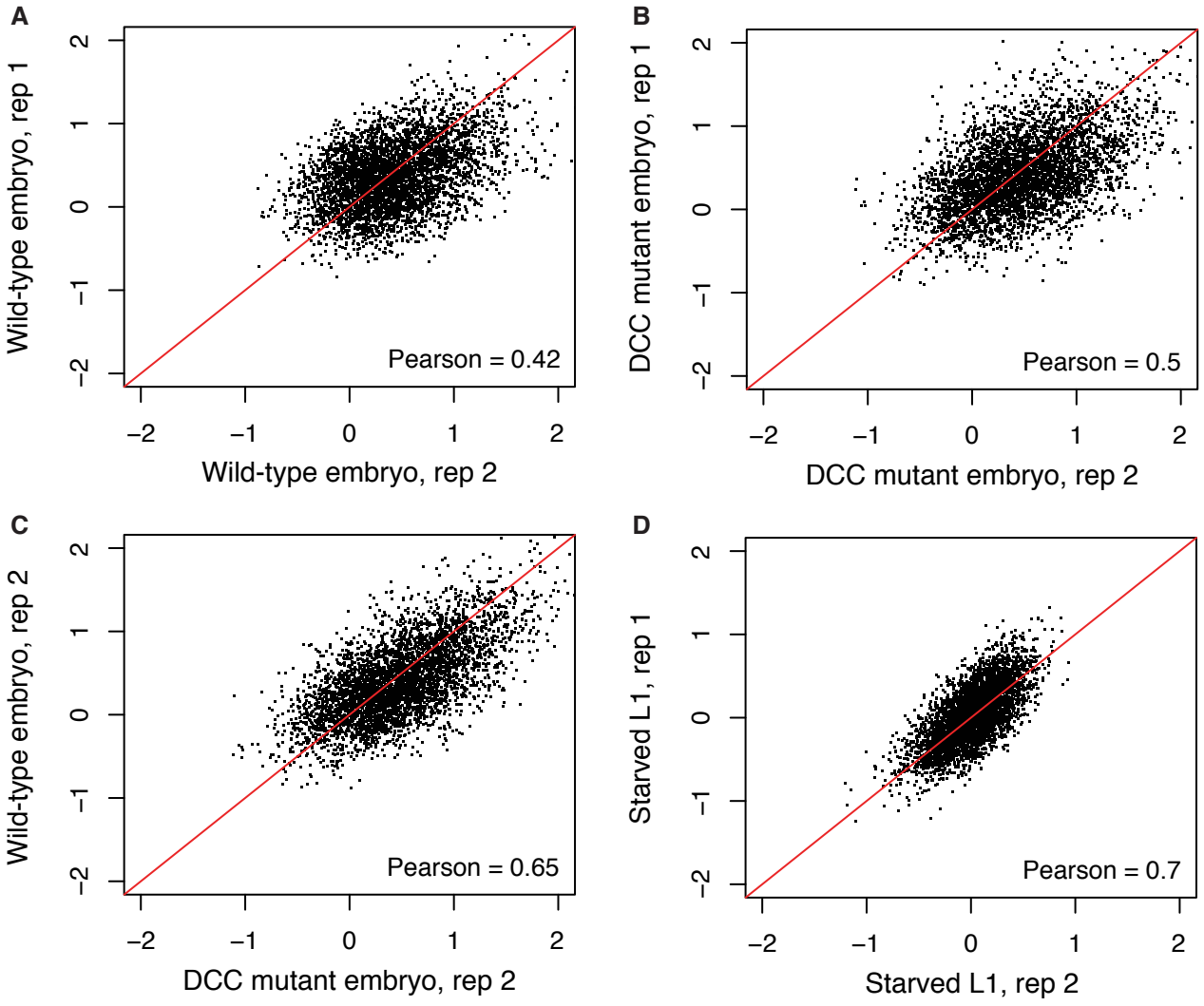

Supplemental Figure S10. Pearson's correlation between BP-seq datasets of wild-type or DCC

mutant embryos and starved L1 larvae. (*A*)-(*D*) Total BP signal was calculated in 500 bp windows around TSSs of highly transcribed genes. The correlation between samples is indicated by the Pearson's correlation coefficient.

Pearson correlation between pairwise combinations of SS-seq datasets in 100 bp windows around TSSs of 4246 genes analyzed in Figure 6A and around TASs and corresponding TESs for 9918 genes with TASs ≥ 50 bp from TSSs

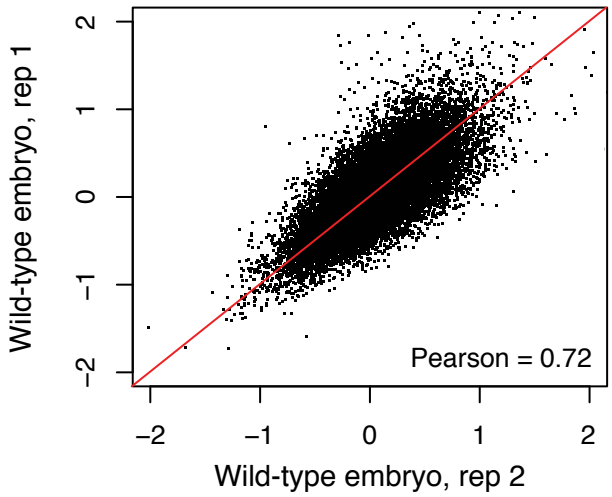

Supplemental Figure S11. Pearson's correlation between SS-seq datasets.

Total SS-seq signal was calculated in a 100 bp window around TSSs of highly transcribed genes and around TASs and TESs of genes with TASs at least 50 bp away from TSSs. The correlation between samples is indicated by the Pearson's correlation coefficient.